

Simulation of tip leakage flow around partial squealer rims in axial turbines

Levent Kavurmacioglu
 Debashis Dey
 Cengiz Camci

Abstract: The present investigation deals with the aerodynamic visualization of tip leakage flow from “partial-length squealer rims” that are constructed separately on the suction side in a single stage turbine rig. After describing the static pressure field on the tip surface with a squealer rim, the vortical flow features around the squealer rim and inside the tip gap are visualized in vertical planes. The leakage flow paths under the control of squealer rims are described in various planes parallel to the blade tip platform on which the squealer rims are attached. Turbine exit total pressure as calculated from the numerical model is presented for the baseline tip and tips with squealer rims. It is clearly shown that a partial squealer rim arrangement can be extremely effective in weakening the tip leakage vortex in a turbine facility provided that the squealer rim height is specified correctly. The study shows that the chordwise length of partial squealer rims near the suction side corner does not significantly affect the desensitization process. The aerodynamic benefits of using a partial squealer tip arrangement located near the suction side of the tip platform in a turbine stage is demonstrated.

Keywords: tip leakage flow, turbine, CFD, flow visualizations, squealer tip.

Biographical notes:

L. Kavurmacioglu received his PhD in Mechanical Engineering from Istanbul Technical University in 1996. He is an Assistant Professor at the Faculty of Mechanical Engineering at Istanbul Technical University, Turkey. His current research interests include flow and heat transfer in Turbomachinery, transient flow and surge in turbomachinery systems. He is presently a Visiting Professor in the Aerospace Engineering Dept. of the Pennsylvania State University.

D. Dey received his Ph.D. in Aerospace Engineering from Penn State in 2001. His doctoral research included turbine tip leakage mitigation in high pressure stages. Currently he is a combined cycle performance test engineer at General Electric, based at Schenectady, NY

C. Camci is a Professor of Aerospace Engineering at the Pennsylvania State University. He obtained his doctoral degree from the von Karman Institute for Fluid Dynamics in Belgium in 1985. He directed research in the Turbomachinery Aero-heat Transfer Laboratory at Penn State since 1985. He teaches theory of turbomachinery, fluid dynamics, turbulent flow, aerospace propulsion and finite element methods in fluid dynamics and heat transfer.

1 INTRODUCTION

1.1 Tip Clearance Flow around a Squealer Tip

The function of a conventional squealer tip design as a turbine tip desensitization arrangement is three fold. The squealer tip provides an effective reduction in tip leakage flow. This approach also protects the blade tip from the full impact of high temperature leakage gases when the squealer tip cavity is also used as a cooling system

component. A third function of this design approach is its protective ability against incidental rubs. *A single surface squealer tip* can be obtained by extending the pressure surface shell from the blade tip platform in radially outward direction. The same approach can equally be implemented as a suction surface extension in radially outward direction. *A double squealer* configuration can be formed by extending both pressure and suction surfaces. This approach results in an enclosed cavity over the blade tip as shown by (Anderson, 1979). This may actually be considered as a simple labyrinth seal

configuration between the turbine casing and rotating blade tip (Wisler, 1985) defines the squealer tip as a method of reducing the possible contact area between the tip and the casing. The main purpose of the squealer tip arrangement is to protect the blade tip and cooling system from smear damage. This is a way of obtaining tighter design clearance in the tip gap region. (Heyes et al., 1992) studied two squealer tip configurations in a cascade configuration and compared these to a flat baseline tip configuration. He showed the potential of squealer tip geometry to reduce tip clearance loss convincingly. Variations of known squealer tip configurations may provide excellent aerodynamic seal systems for the turbine tip gap region. As the designs become more elaborate they may also become more difficult and expensive to manufacture. A 2D computational tip gap model using Navier Stokes equations was used by (Chen, Dawes and Hodson, 1993) in the calculation of leakage discharge coefficients for various squealer tip arrangements. The implementation of chordwise sealing strips on a turbine tip surface was presented by (Bunker et al., 2000). An experimental and numerical heat transfer investigation of a turbine tip section with a mean camber-line strip was investigated by (Ameri, 2001) for a large power generating turbine. A radiused edge tip and a sharp edge tip was investigated with a mean camber-line strip on the tip surface. The favorable conditions created by using a sharp edge tip are explained. Effects of a squealer tip covering the complete perimeter on rotor heat transfer and efficiency was investigated in a numerical simulation by (Ameri, Steinhorsson and Rigby, 2000).

1.2 Current objectives:

The present investigation deals with the aerodynamic visualization of tip leakage flow from “partial-length squealer rims” that are constructed separately on the suction side in a single stage turbine rig. The computational visualizations obtained from three dimensional turbulent flow simulations using a general purpose RANS solver are interpreted using recent aerodynamic field measurements that are obtained in a rotating turbine facility (AFTRF). The details of the turbine facility and the recent measurements using partial squealer tips are presented in (Camci, 2004), (Lakshminarayana, Camci, Halliwell & Zaccaria, 1992) and (Camci, Dey and Kavurmacioglu, 2003). Current results indicate that the use of “partial squealer” arrangements can positively affect the local aerodynamic field by weakening the leakage vortex. Visualizations clearly show that the suction side partial squealer rims are capable of reducing the aerodynamic losses associated with the leakage flow to a significant degree. A comparison of the numerically visualized tip gap flow field and measured aerodynamic field in the turbine suggests that RANS simulations are effective in explaining local three dimensional flow details in turbine flow zones in which aerodynamic measurements are

difficult to perform. Numerically generated “surface oil flow visualizations” on the tip surface and numerically generated vortical flow details on user defined planes (numerical equivalent of laser sheet visualizations) can be effectively used to discuss local tip flow physics. The study also shows that the turbine tip surface includes many different leakage flow regimes depending upon the effective tip clearance, the specific tip platform geometry, local loading conditions and the rotational speed of the rotor.

2 NUMERICAL ANALYSIS

The three-dimensional, steady, turbulent form of the Reynolds-averaged Navier Stokes equations are solved for the detailed visualization of complex turbine passage flow in AFTRF .A two equation turbulence model from (Lauder and Spalding, 1974) using the transport equations for the turbulent kinetic energy and the turbulent dissipation rate are used for the determination of local turbulent viscosity in the domain,. The governing equations, the turbulence model, the near wall treatment, the method of solution, the boundary conditions used in the numerical procedure and the grid structure are explained in an earlier paper by (Kavurmacioglu, Dey and Camci, 2004). Figure 1 shows the grid system used for the calculations near the squealer rim region and a baseline tip grid without a squealer rim. The inlet boundary conditions used for the computational effort are specified by using the measured mean velocity and turbulence intensities at just upstream of the turbine rotor in AFTRF. Details of the measured turbine rotor inlet flow conditions and their comparison to design values for the stage are presented in (Kavurmacioglu, Dey and Camci, 2004).

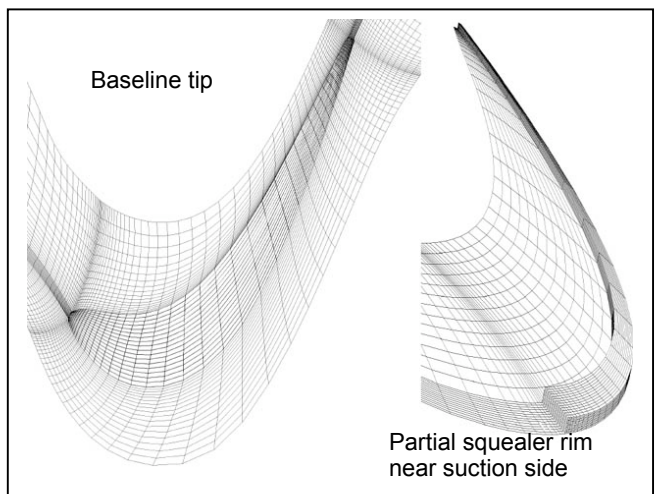


Figure 1, The grid system used for the calculations near a baseline tip and the squealer rim region

SIMULATION OF TIP LEAKAGE FLOW AROUND PARTIAL SQUEALER RIMS IN AXIAL TURBINES

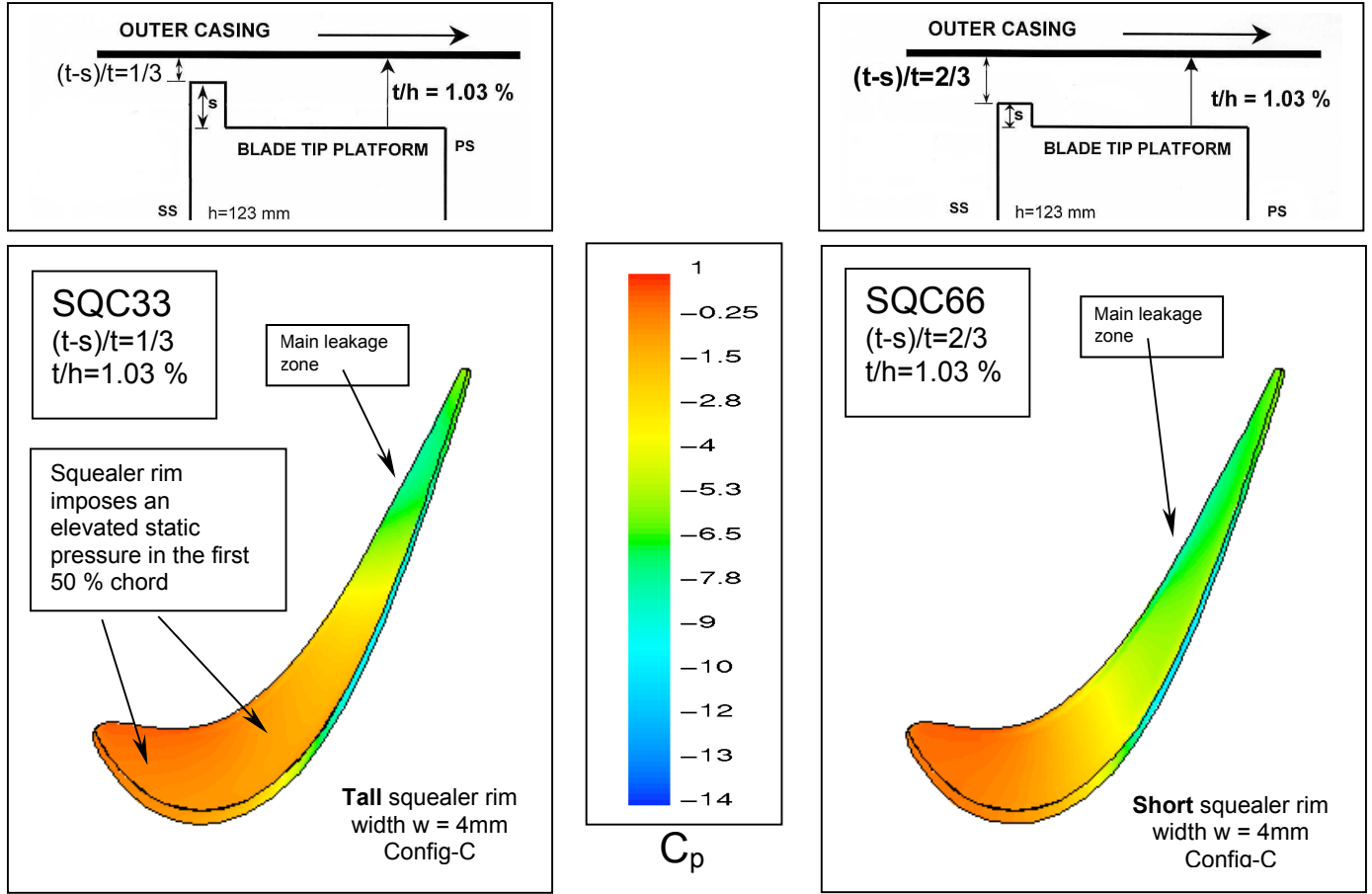


Figure 2 Static pressure distribution on the tip surface with a partial squealer tip arrangement on the suction side

2.1 Effective Clearance Height ($t-s/t$) for Partial Squealer Rim Design:

Figure 1 shows one of the three partial squealer rim arrangements presented in this paper. The specific squealer rim termed "Config C" that has a constant rim width of $w=4$ mm starts from the leading edge and ends at the trailing edge. $(t-s)/t$, s being the height of the squealer rim is a termed as the "effective clearance height" throughout this paper. The non-dimensional effective gap $(t-s)/t$ between the top surface of the squealer rim and the outer casing is the most critical geometrical parameter in the design of a partial squealer rim. The distance between the blade tip platform and the outer casing t/h is fixed to the value used for the baseline case BS100 ($t/h=1.03\%$) for all partial squealer designs (Config A, Config B and Config C). Config A, B and C are only different because of their chordwise length. Our baseline study without squealer rims presented in (Kavurmacioglu, Dey and Camci, 2004) shows that, there is a significant amount of tip leakage for BS100 ($t/h=1.03\%$). One can reduce this leakage flow by designing an extremely tight tip gap such

as the case BS33 ($t/h=0.33\%$) as previously discussed. However, $t/h=0.33\%$ operation may be difficult to maintain in an actual engine environment. The aerodynamic performance of BS33 is exceptionally good with minimized leakage vortex development. The main strategy in designing partial squealer tips is to use a tight gap "only" on top of the squealer rim. This tight space is termed as "*effective clearance height*" $(t-s)/t$ as shown in Figure 2. The difference between SQC33 and SQC66 is only in the height of the "*effective tip gap height*". $(t-s)/t$ in SQC33 is only 33% of the tip gap t (or $t/h=1.03\%$). $(t-s)/t$ in SQC66 is 66% of the tip gap t . The aim in designing the partial squealer tip is to generate minimized leakage flow conditions that are similar to BS33. However the tight clearance space $(t-s)/t$ is only applied to only a $w=4$ mm wide tiny squealer strip. The blade needs to have a comfortable clearance t/h in a wide area on the tip platform. An extremely narrow band ($w=4$ mm) of squealer rim serves as a chordwise sealing strip near the suction side allowing the tip to continue its sustainable operation even under rubbing conditions.

2.2 Static Pressure Field on the Tip Surface with Squealer Rims:

The static pressure distribution on the tip surface with a partial squealer rim (Config-C) is shown in Figure 2. The same color band previously used in Figure 5 of (Kavurmacioglu, Dey and Camci, 2004) is used in order to facilitate easy comparison of the squealer tip pressure distribution against the baseline tip configurations BS100 and BS33. Although a squealer rim occupies a small portion of the blade tip platform, it has the ability to significantly modify the static pressure distribution of the comparable baseline case. SQC 33 configuration in Figure 2 has the same t/h value as the BS100 shown in Figure 5 of [21]. However, $(t-s)/t$ assigned to the zone above the narrow squealer rim is about 1/3 of the larger gap $t/h=1.03\%$, as shown in Figure 3. The static pressure on the blade tip platform of SQC33 is at a significantly higher level in the first 50% chord length distance from the leading edge. The low momentum region indicated by red-yellow zone is usually related to minimal leakage activity on tip surfaces. The blue zone noted as the highest leakage area on BS100 does not exist on SQC33 blade tip platform. The restrictive barrier influence of the squealer rim is apparent when the top surface of the rim is examined from static pressure point of view. This narrow flow area characterized by $(t-s)/t$ develops a relatively lower local pressure when compared to its identical chordwise locations on the blade tip platform. The blue-green zone on the narrow rim top surface is an indication of the acceleration of the leakage flow in an extremely tight and effective gap. The pressure differentials in a direction normal to blade camber line are minimal in the first 20 % chord of the tip surface where the high pressure zone occurs (red-yellow area). The trailing edge region in the last 20 % of the chord also experiences similar static pressures (green zone in Figure 2) on the concave and convex sides of the blade contour.

2.3 Velocity Field in Planes Parallel to Tip Platform (with squealer rim):

Figure 3 shows the velocity vectors in the lower z/t plane and higher plane for two different effective squealer heights using the longest squealer rim termed Config C. In SQC66 which is for the short squealer rim (top two figures), the lower visualization plane at $z/t=1/3$ indicates a weakened tip vortex formation when compared to BS100. It is also apparent from dominantly blue vectors that the leakage flow direction in the first 20 % chord distance is from the leading edge to mid chord location. Significant transfer of fluid from the pressure side to suction side (or vice versa) is not induced in this leading edge area. The influence of the squealer rim appears as “a better channelling of the tip leakage flow” into a more chordwise direction. This channelling effect is more apparent in the visualization plane near the tip platform ($z/t=1/3$). The blue velocity vectors (lowest velocity magnitude) near the pressure side tend to move into the

leakage vortex. It should be noted that $z/t=1/3$ visualization plane passes through the first grid point existing over the rim top surface on which no-slip condition is imposed. The dominant leakage zone existing in BS100 between the 50% and 80% locations appears to be weakened in SQC66. The results from SQC33 configuration (tall squealer) are shown in the lower row of Figure 3. The flow channelling effect of the squealer rim with a $(t-s)/t=1/3$ creates velocity vectors tending to follow the curvature of the squealer rim in the chordwise direction after the first 20 % chord distance from the leading edge. A considerably weakened tip vortex is visible near the suction side. The leakage flow reverses in the trailing edge wedge area as indicated by blue vectors that have comparable momentum to the leakage fluid in the leading edge area. The flow reversal is more apparent in the higher visualization plane $z/t=5/6$ very near the trailing edge radius. The leakage flow reversal near the trailing edge is the direct result of the viscous/turbulent shear forces imposed by the outer casing relative motion. The shear effect usually dominates the tip gap flow in regions where the driving pressure differential along the leakage pathlines is minimized by the specific loading character of the blade tip.

2.4 Re-circulatory Tip Flow Patterns in Cross-Stream Planes (with squealer rim):

Figure 4 presents the leakage vortex de-sensitization capability of squealer rims for $(t-s)/t=2/3$ and 1/3. The results for SQC66 (short squealer rim) shows similar qualitative trends when compared to the baseline case BS100 as shown in Figure 7 of reference (Kavurmacioglu, Dey and Camci, 2004). A leakage flow from the pressure side to suction side in plane X creates a relatively weaker leakage near the suction side corner when compared to BS100. In plane Y, a significant amount of fluid leaks to the suction side. When plane Z is reached, the tip gap flow guided by the squealer rim corner starts to send a portion of the leakage flow back to the pressure side. A small separation bubble on the top surface of the rim is also apparent. In plane T near the trailing edge, the leakage flow is now completely reversed to the pressure side. In almost all tip simulations, a very stratified pathline structure on the tip platform is observed when the flow is completely reversed to the pressure side. A significant driving force for the near trailing edge leakage seems to be the viscous/turbulent shear forces imposed by the motion of the outer casing.

The “tall squealer rim” results for the full length squealer rim (Config-C) are also shown in Figure 4. $(t-s)/t=1/3$ for SQC33. The blade tip gap is $t/h=1.03\%$. An effective tip de-sensitization is observed due to relatively small effective clearance height. The tip vortex forming at location X is much smaller than the vortex observed for SQC66 (short rim) presented on the left column of Figure 4. The size of the vortical zone at X is comparable to the baseline tip BS33 that achieves similar de-sensitization

SIMULATION OF TIP LEAKAGE FLOW AROUND PARTIAL SQUEALER RIMS IN AXIAL TURBINES

levels. The cross stream plane pathlines at Y show a complicated re-circulatory flow pattern mainly because of the flow angle variations observed in various z/t planes located between the blade tip platform and outer casing. As the fluid guided/trapped near the concave side corner of the rim leaks into the suction side, there is a significant amount of leakage fluid directed to the pressure side, because of the strong outer casing shearing effect (middle vortex with clockwise rotation). There is also a third re-circulatory flow zone (counter clockwise) located near the pressure side corner. This entry zone structure is clearly influenced from the specific cross flows in the core of the turbine passage and the static pressure distribution on the tip platform as defined by the squealer rim. The flow near the pressure side corner makes an attempt to enter the tip gap, however the viscous/turbulent shear forces imposed by the outer casing has the capability to pull some of this flow into the near wall zone of the outer casing in plane Y. There is a counter clockwise rotating re-circulatory flow zone at just downstream of the pressure side corner. The SQC33 (tall rim) leakage character in plane Z is qualitatively very similar to SQC66. The leakage flow near the rim top surface sends a small amount of fluid into the weak tip vortex structure. Some of the fluid near the rim surface is also turned towards the pressure side on the tip platform surface. A complete flow reversal for SQC33 inside plane T occurs very similar to SQC66. However, the strong tip vortex that is feeding into the tip gap zone observed in SQC66 does not exist in plane T of SQC33. Figure 4 clearly demonstrates different leakage flow patterns around squealer rims resulting from the balance of pressure forces, viscous/turbulent shear forces and inertia forces related to convective accelerations along leakage flow paths.

2.5 Leakage Flow Patterns in Planes Parallel to Tip Surface (With Squealer Rim):

Figure 5 shows the influence of squealer rim on the leakage pathlines, in planes parallel to tip platform in the gap region. The short rim (SQC66) pathlines (upper row) in higher plane show a sizeable tip vortex formation. The leakage feeds into the tip vortex in the first 30% chord length fluid from the suction side corner. When the pathlines are visualized in the lower visualization plane, a channelling effect of the squealer rim near the leading edge and trailing edge is observed. A part of the leakage flow in the lower plane is diverted into the wake region near the trailing edge before it finds a chance to cross the squealer rim structure in the usual leakage direction from the PS to SS. When the pathlines for the tall rim (SQC33), a stronger outer casing effect near the leading edge is visible for higher plane $z/t=5/6$, (lower row in Figure 5). In the first 30 % chord near the leading edge, as some suction side fluid is directly passing towards the pressure

side, some of the fluid is diverted back into the tip vortex near the suction side corner. The leakage fluid near the trailing edge also deviates towards the pressure side. The turning of the pathlines belonging to tall rim (SQC33), ($z/t=5/6$) from the suction side towards the pressure side is visible in Figure 5. The pathlines in the lower plane clearly demonstrate the flow dividing effect of the squealer rim. The leakage fluid trapped in the gap region is channelled towards the trailing edge near the concave corner of the squealer rim. The leakage fluid channelled towards the trailing edge and the relatively weak tip vortex material tend to be deflected towards the pressure side near the trailing edge point.

2.6 Influence of Tip Gap Height on Stage Exit Total Pressure (Baseline Tip):

Figure 6 shows the contour plots of stage exit total pressure coefficient C_{po} for the two baseline cases (BS100 and BS33). The visualization plane E is defined as the plane normal to streamwise flow direction at 30 % chord downstream of the trailing edge. A sketch showing the exact location of plane E is given in Figure 3 of (Kavurmacioglu, Dey and Camci, 2004). The results from the two squealer tip configurations (SQC33 and SQC66) are also presented in Figure 6. The dark blue color is assigned to the lowest level of calculated total pressure appearing at the core of the tip leakage vortex BS100 located in the last 15-20 % of the blade height. The wake of the blade and its interaction with the tip vortex is apparent. The change in the mass averaged total pressure coefficient (\bar{C}_{po}) over visualization plane E is about -3.56 for the baseline blade tip configuration BS100 ($t/h=1.03\%$).

The contour plot of stage exit total pressure coefficient C_{po} on plane E for the tight baseline clearance case BS33 shows a dramatic improvement in stage exit aerodynamic field. The yellow and green dominated core flow zones of BS100 are converted into red-yellow zones with significant aerodynamic gain in BS33. The highest computed total pressure is denoted by red in Figure 6. This configuration belonging to BS33 shows a dramatic improvement of the aerodynamic field all over the exit plane. The reduction in the size and strength of the tip vortex is clearly visible in the contour plot. The passage vortex is not totally washed away by a strong tip vortex. The interaction of the weak tip vortex is apparent. This case was only obtained just to see the overall influence of a leakage vortex on the stage exit total pressure field. Daily turbine operation with such a tight clearance ($t/h=0.33\%$) may not be practical. There is a dramatic drop in the level of mass averaged aerodynamic loss coefficient assigned to relative flow in the passage. \bar{C}_{po} for BS33 is -2.11.

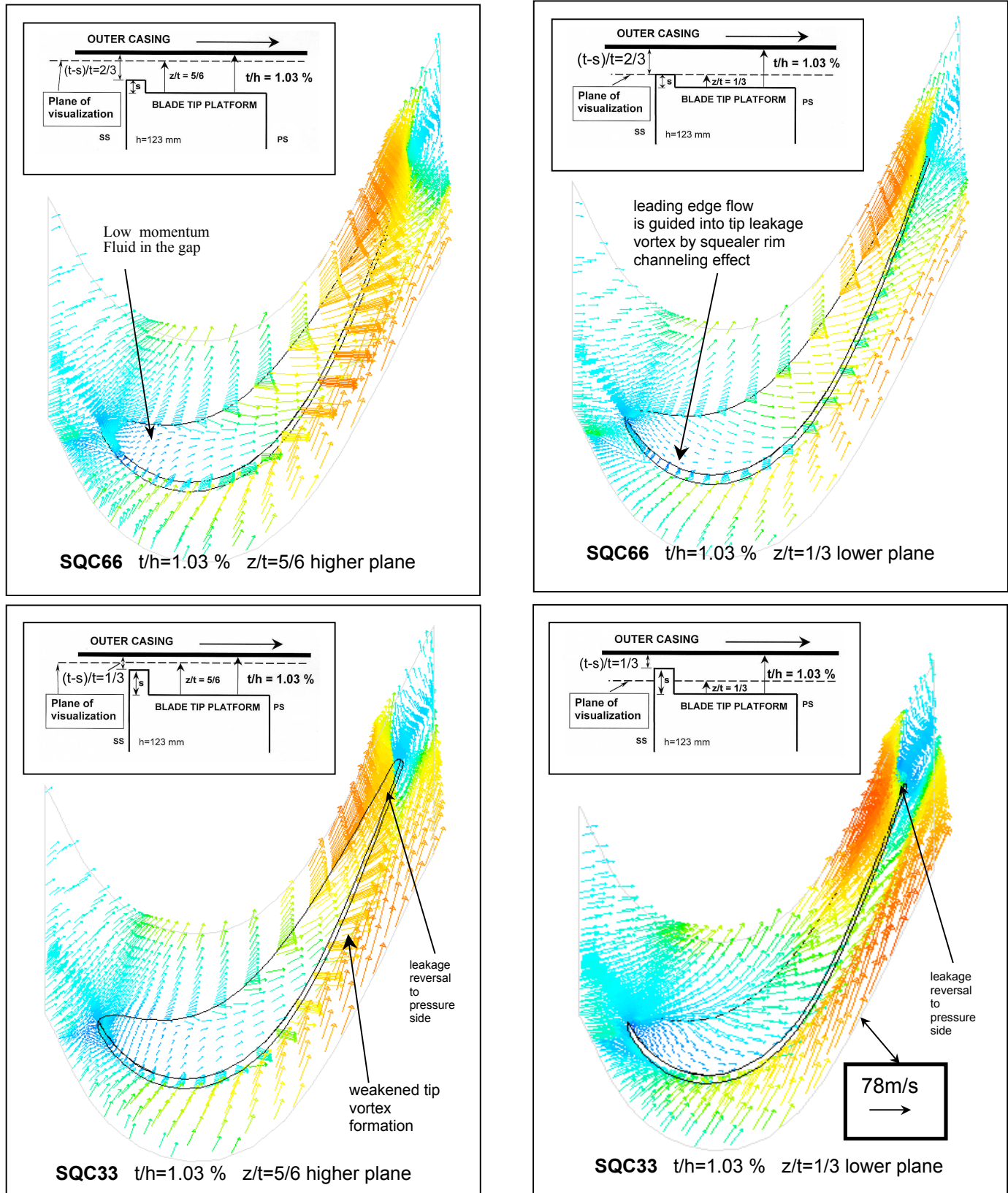


Figure 3 Leakage flow patterns in planes parallel to the tip surface, (PARTIAL SQUEALER TIP, Config C)

SIMULATION OF TIP LEAKAGE FLOW AROUND PARTIAL SQUEALER RIMS IN AXIAL TURBINES

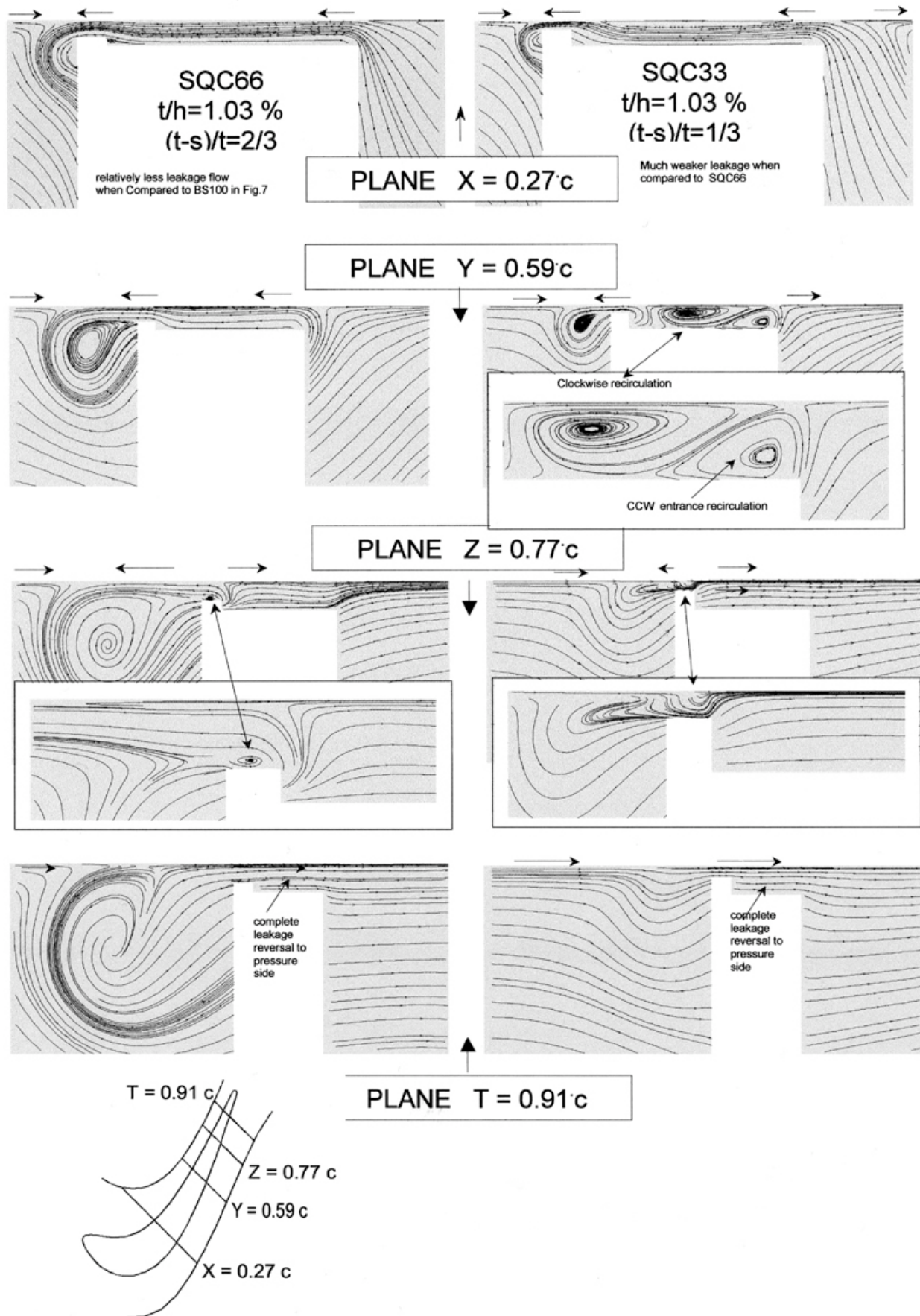


Figure 4. Leakage flow patterns in the tip gap space inside cross stream planes (PARTIAL SQUEALER TIP ON THE SUCTION SIDE), Config C, FULL LENGTH

The detrimental effect of having a strong tip vortex in the passage is demonstrated in this figure. The rest of the passage can attain a higher total pressure when the baseline clearance is tighter (BS33) because of the weakened tip vortex flow.

2.7 Influence of Tip Gap Height on Stage Exit Total Pressure (Partial Squealer Tip, Config-C):

The “tall” squealer tip configuration SQC33 with a rim extending from the leading edge to trailing edge is also presented in Figure 6. For this case, the effective clearance height ($t-s$) between the rim top surface and the outer casing is the same as the tip clearance of the baseline tip with $t/h=0.33\%$ (BS33). The clearance on tip platform areas (other than the rim top surface) is $t/h=1.03\%$ (the same as BS100). The corresponding $(t-s)/t$ is $1/3$ over the rim top surface. The total pressure field on surface E is very similar to the result from BS 33. Having the same effective clearance height as the case BS33 results in a very similar exit flow structure. The aerodynamic benefits of the extreme case BS33 can be easily obtained from a more practical squealer configuration as shown for SQC33. The relative change in mass averaged total pressure coefficient for this case is $\Delta C_{po}=-1.97$.

When the effective clearance height $(t-s)/t$ is increased to $2/3$ for the same $t/h=1.03\%$, the effective flow area in the leakage zone is doubled. This is achieved by reducing the rim height s for comparison purposes. t/h for SQC33 and SQC66 is the same, however the rim height s in SQC33 is doubled when compared to that of SQC66. The fourth contour plot in Figure 6 indicates a relative increase in the size of the tip leakage vortex in plane E. However the total pressure in the core of the tip vortex is not as low as the baseline case BS100. Although the tip leakage vortex occupies almost the same area as the case BS100, its total pressure defect is clearly eliminated for SQC66 because of the barrier effect created by the squealer rim. The rest of the passage is dominated by red-yellow high total pressure fluid when compared to that of BS100. In BS 100, the areas outside the tip vortex are dominated by a yellow-green intermediate total pressure areas. When the whole exit plane is considered, the mass averaged total pressure coefficient for SQC66 is about $\Delta C_{po}=-2.22$.

For the longest squealer rim Config-C, the “tall rim” SQC33 and the “short rim” SQC66 provides excellent tip de-sensitization levels ($\Delta C_{po}=-1.97$ and -2.22). The “short rim” ΔC_{po} level is very close to the tight baseline case BS33 ($\Delta C_{po}=-2.11$). Both of these squealer tip configurations are excellent aerodynamic alternatives to the equivalent baseline tip BS100 with a flat tip.

2.8 A Comparison of the Exit Total Pressure at Radial Positions Near the Tip Region:

Figure 6 also presents the variation of total pressure along the cross stream direction in plane E at radial positions $r/h=79.3\%, 89.7\%, 92.2\%$ and 94.8% . The 79.3%

location is the location where the tip leakage effects are still felt in BS100. BS100 represented by the solid line produces the largest total pressure drop in all four radial positions. When the results for BS33 are examined, the dashed lines in all four radial positions show the dramatic influence of closing the tip gap height.. Significant gains in total pressure are visible in all four radial locations when the dashed line is compared against the solid line of BS100. The width of the total pressure defect zone is also significantly reduced. The results for SQC33 are represented by stars in the line distributions of total pressure coefficient. SQC33 (the tall rim) total pressure defects are very comparable to BS33 (tight baseline) in terms of the level and the area coverage, suggesting that the leakage flow field near the suction side corner is very similar in SQC33 and BS33. This feature is also apparent in the contour plots. SQC66 (short rim) performs somewhere between the baseline case BS100 (baseline with flat tip) and BS33 (tight baseline).

2.9 Influence of Squealer Rim Length on Stage Exit Total Pressure (Config-A, Config-B and Config-C):

The contour plots for the stage exit total pressure coefficient in plane E and the line plots of the total pressure coefficient in cross stream direction for the three squealer tip lengths investigated are given in Figure 7. All three configurations produce very similar mass averaged total pressure coefficients in plane E. Config-C may have a slightly better flow channeling effect since it is extended all the way to the leading edge point. The solid line in scatter plots is for Config-C. The total pressure levels and deficits are very similar for all three squealer rim lengths. The middle length rim Config-B and the shortest rim Config-A produce almost equivalent mass averaged aerodynamic loss coefficients over the exit plane, ($\Delta C_{po}=-2.29$) . The aerodynamic impact of the three squealer rims is possibly in the near wall wake structure of the rims with different chordwise lengths. Near rim boundary layer effects do not seem to be transmitted to the other sections of the exit plane effectively.

2.10 Surface Oil Flow Visualizations on the Blade Tip Surface:

The leakage flow paths near the tip platform for the baseline case and squealer rim cases can be visualized by performing “numerical” surface oil flow visualizations. This post-processing feature tracks the pathlines of massless particles located on the tip platform by considering the magnitude of the wall shear stress and its direction in a Lagrangian trajectory calculation.

The baseline case BS100, the shortest squealer rim SQA33 (Config-A) and the longest squealer rim SQC33 (Config-C) are presented in Figure 8 for $t/h=1.03$. The surface oil flow lines in the first 20 % chord of the blade

SIMULATION OF TIP LEAKAGE FLOW AROUND PARTIAL SQUEALER RIMS IN AXIAL TURBINES

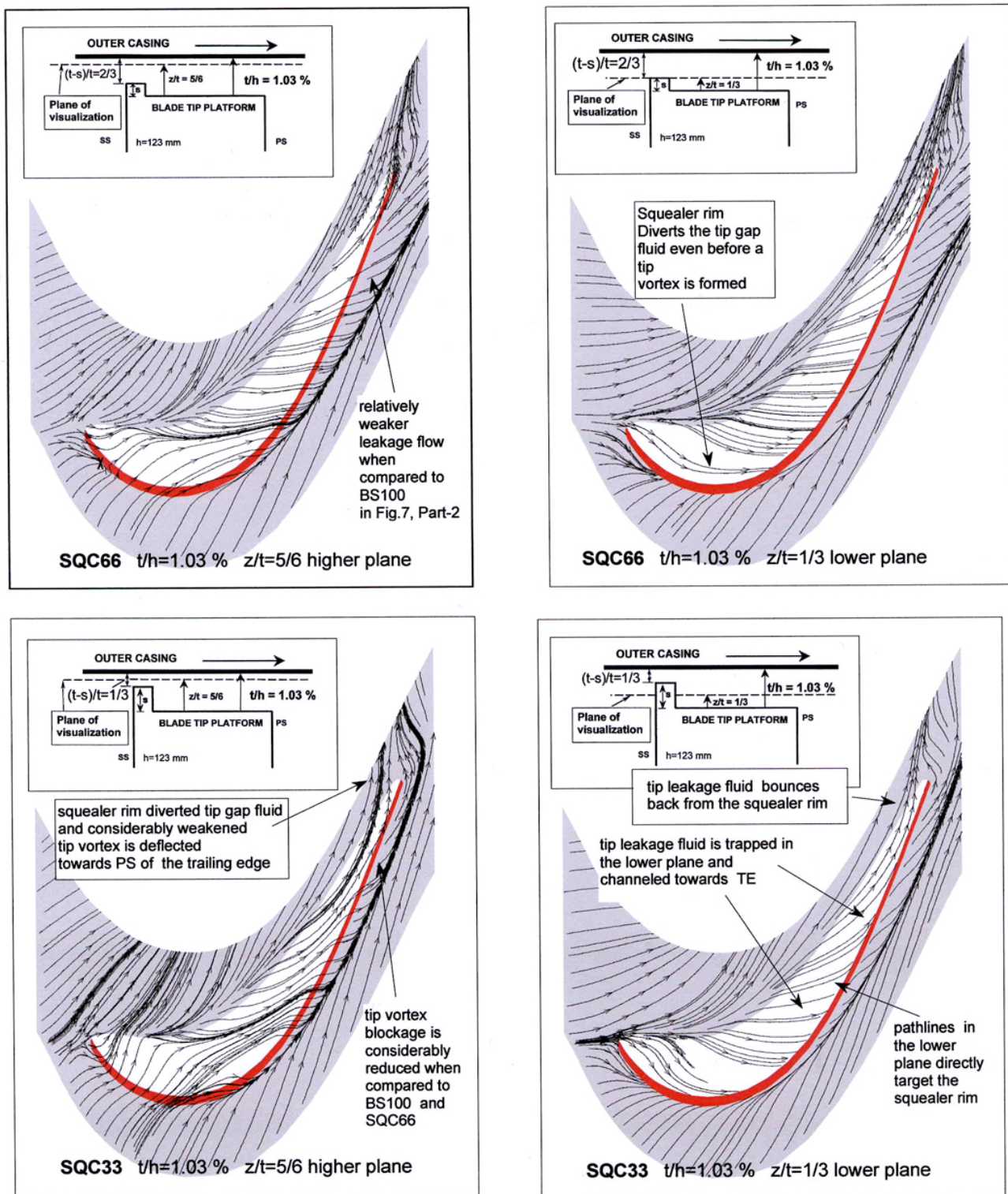


Figure 5 Leakage flow patterns in planes parallel to the tip surface(PARTIAL SQUEALER TIP ON THE SUCTION SIDE), Config C, FULL LENGTH

mainly originate from a central point very near the stagnation point. It seems, most of the fluid in the region corresponding to low momentum activity originate from a near stagnation point location on the tip platform. In strong leakage areas, the oil flow lines clearly show the leakage flow paths between the PS and SS. Near the trailing edge, the oil flow lines tend to turn towards the pressure side slightly because of the outer casing shear effects discussed in this paper.

The shortest squealer rim termed Config-A shows considerably different surface oil flow visualization. The oil flow lines near the leading edge favor to cross this zone from the pressure side to suction side. However, the momentum of the leakage fluid in this zone is considerably low. The squealer rim clearly diverts the fluid near the tip platform starting from the leading edge of the rim. The accumulation of the tip gap fluid on the concave side of the rim on the platform surface is visible in Figure 8. The squealer rim deflects the leakage fluid back to the pressure side in the last 20% chord of the blade. The deflection of the oil flow lines back to the pressure side is consistent with the gap flow visualizations in the trailing edge wedge zone as shown in Figure 5.

The leakage flow control effects of the longest rim Config-C is very similar to the shortest squealer rim Config-A. This observation made from oil flow visualizations is consistent with the mass averaged aerodynamic loss coefficients for the stage exit plane E. It seems the leakage fluid in the near leading edge area (first 20 % chord) will not effectively alter the structure of the tip leakage vortex that forms near the suction side corner.

3. CONCLUSIONS

The experimental results from an experimental program explaining the aerodynamic structure of a baseline tip and various squealer tip configurations in a turbine research facility were given in Part-1. A detailed numerical visualization of the same tip leakage flow around a baseline tip in AFTRF was also presented in Part-2. The numerical visualizations obtained from a solution of the 3D, steady and turbulent Reynolds-averaged Navier-Stokes equations formed a basis for detailed leakage flow visualizations for baseline tip configurations in AFTRF. This paper focuses on the flow physics around partial squealer tip arrangements for effective tip de-sensitization. The existence of a partial squealer rim on the tip platform of a turbine blade significantly modifies the tip surface static pressure distribution.

The squealer rim channels the leakage fluid in a chordwise direction in such a way that the leakage fluid passing to the suction side of the blade is minimized. A clear barrier influence of the squealer rim was shown for two practical rim heights.

The two squealer tip effective clearances are investigated for $(t-s)/t=1/3$ and $(t-s)/t=2/3$ for the longest rim. SQC33 and SQC66 provided a dramatic improvement in mass averaged aerodynamic loss coefficients when compared to the baseline tip BS100. Complete reversal of the leakage fluid near the trailing edge of the blade is possible when a squealer rim is used. This reversal feature is also observed in the baseline leakage flow field.

The visualizations based on linear momentum equation in the turbine passage show that the viscous/turbulent shear effect from the relative motion of the outer casing can be dominant in the regions where the driving pressure differential is minimized along the leakage flow paths in the gap. The aerodynamic structure of the tip leakage flow is severely influenced from the outer casing motion in a turbine stage. The leading edge leakage flow occurs with relatively low momentum and most of the tip gap fluid in this region finally merges with the relatively weak leakage vortex of the squealer rim configuration.

The fluid trapped in a tip vortex on the suction side part of the channel can go back to the tip gap especially near the trailing edge even for the squealer tip configuration (Figure 4). The same feature for the baseline tip was observed.

The highest level of the aerodynamic loss was observed in the baseline tip configuration with $t/h=1.03\%$ (BS100). The existence of a strong tip vortex for this case affects the complete passage. The mass averaged aerodynamic loss coefficient obtained from the baseline tip configuration BS100 indicates the highest level of passage averaged loss when compared to the tight clearance baseline case (BS33), and the two squealer tip cases (SQC33 and SQC66).

The implementation of a squealer tip configuration produces a much weaker tip vortex core on the suction side of the blade when compared to a baseline case. The weakening of the tip vortex is felt over the whole passage from the hub to the outer casing.

For the longest squealer rim Config-C, the extremely tight effective clearance case SQC33 and SQC66 provides an excellent tip de-sensitization level ($\Delta C_{po} = -1.97$ and -2.22). This level is very close to that of the tight baseline case BS33 ($\Delta C_{po} = -2.11$). Both of these squealer tip configurations are excellent aerodynamic alternatives to the equivalent baseline tip BS100 that has no tip de-sensitization on the tip platform.

Three different squealer rim lengths in the chordwise direction are studied for their aerodynamic impact. All three configurations produce very similar mass averaged aerodynamic coefficients when the whole exit plane is considered. Config-C may have a slightly better flow channeling effect since it is extended all the way to the leading edge.

The middle length rim (Config-B) and the shortest rim (Config-A) produce nearly equivalent mass averaged aerodynamic loss coefficients over the exit plane. ($\Delta C_{po} = 2.29$). The aerodynamic impact of the three

SIMULATION OF TIP LEAKAGE FLOW AROUND PARTIAL SQUEALER RIMS IN AXIAL TURBINES

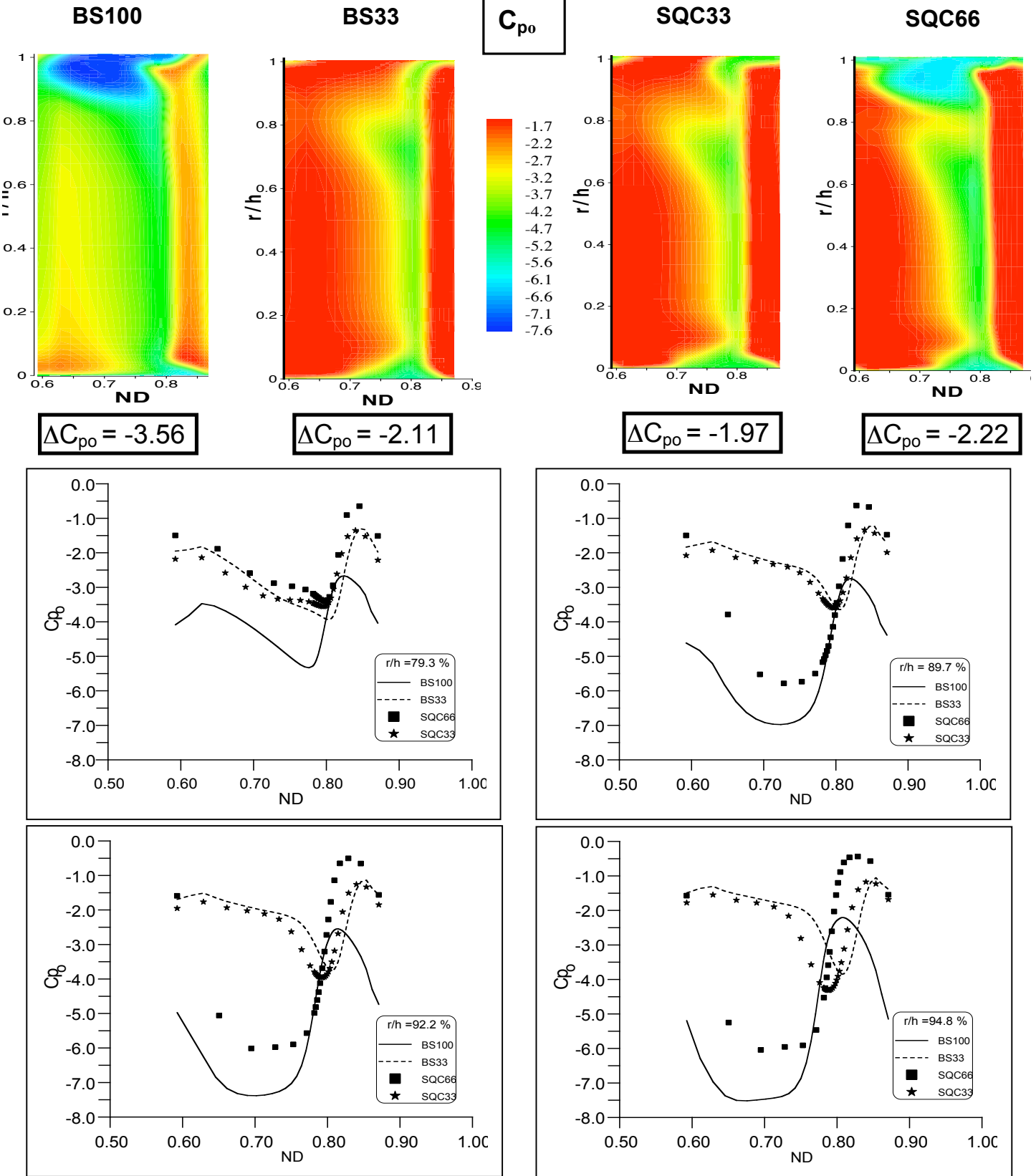


Figure 6 Influence of tip gap height on stage exit total pressure and mass averaged aerodynamic loss coefficient $\Delta C_{po} = (\bar{C}_{po,E} - \bar{C}_{po,inlet})$ baseline tip and partial squealer tip (Config C) on the suction side, plane E

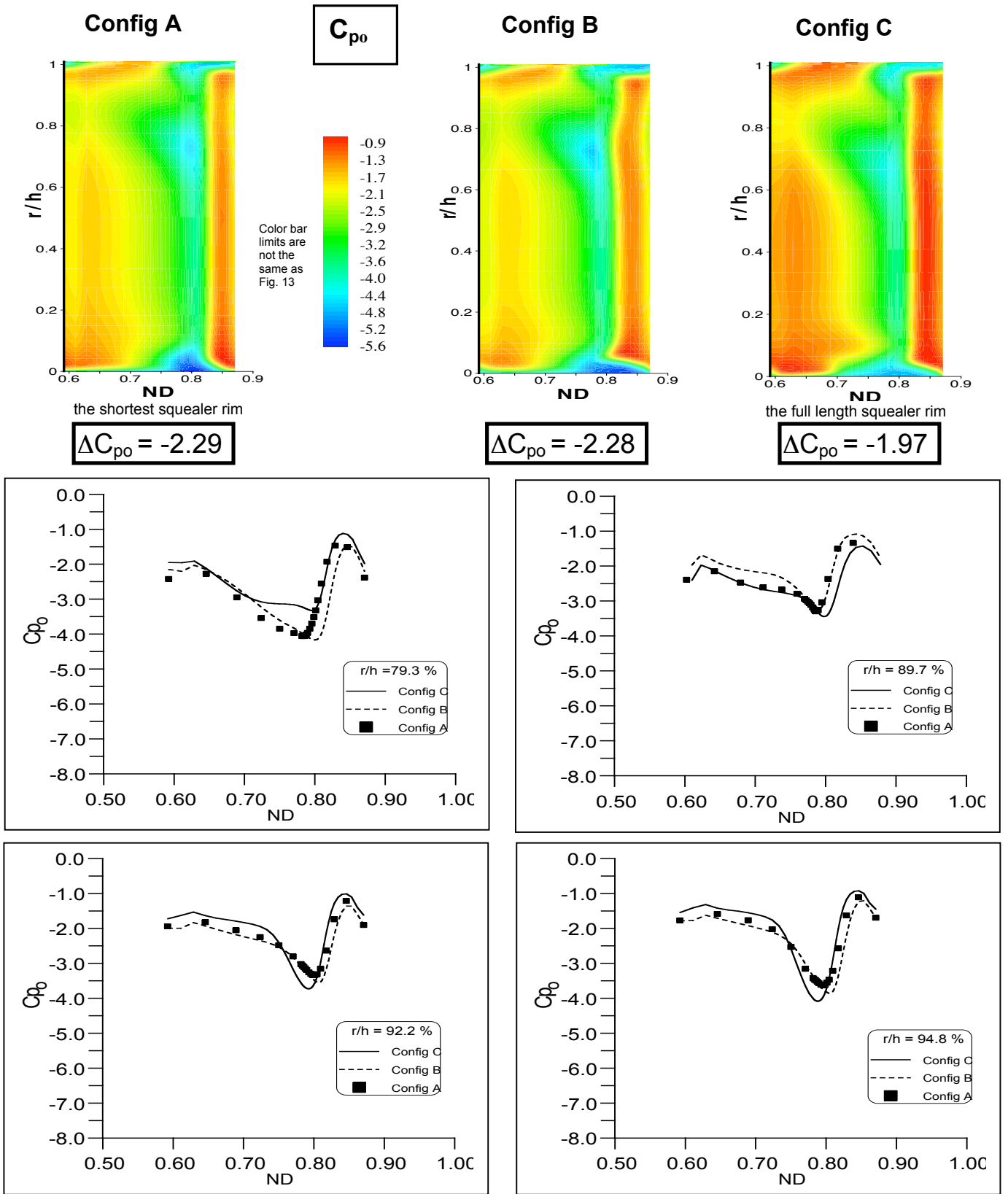


Figure 7 Influence of squealer rim length on stage exit total pressure, and mass averaged aerodynamic loss coefficient
 $\Delta C_{po} = (\bar{C}_{po,E} - \bar{C}_{po,inlet})$ (Config A, Config B and Config C)

SIMULATION OF TIP LEAKAGE FLOW AROUND PARTIAL SQUEALER RIMS IN AXIAL TURBINES

squealer rims is possibly in the boundary layer/wake of the rims with different chordwise lengths.

The leakage flow paths on the tip platform can be visualized by performing “numerical” surface oil flow visualizations with and without squealer rims. The squealer rim guides the leakage flow near its concave surface by minimizing the leakage flow to the suction side.

The surface oil flow visualizations on the platform show that the squealer rim can deflect the leakage fluid back to the pressure side in the last 20% chord of the blade. The outer casing motion provides extra help in pulling the leakage fluid from the suction side to the pressure side.

The numerical visualizations are capable of producing the overall structure of 3-D turbine passage flow including tip vortices for engineering design purposes. Although the quantitative nature of aerodynamic loss coefficients can be questioned in this computational effort, the relative influence of pressure imbalances, viscous/turbulent shear forces, the inertia of convective accelerations are properly represented.

NOMENCLATURE

c	Rotor axial chord length at tip = 0.129 m
BS100	Baseline tip configuration with no tip treatment, full cover , t/h=1.03 % and s=0 mm.
BS33	Baseline tip configuration with no tip treatment, full cover , t/h=0.33 % and s=0 mm.
C_p, C_{p_0}	Static and total pressure coefficients $C_p = (p - p_{ref}) / 0.5 \rho W_{inlet}^2,$ $C_{p_0} = (p_0 - p_{o,ref}) / 0.5 \rho W_{inlet}^2$
E	Flow visualization plane defined at 30 % chord downstream of the trailing edge
h	Rotor blade height = 0.123 m
p_o	Total pressure p_{atm} Ambient pressure (also p_{ref})
p_{in}	Inlet total pressure
p	Static pressure
PS, SS	Pressure side, suction side
Re	Reynolds number
r/h	Non-dimensional radial position measured from hub surface (also y/h in contour plots)
r,θ	Radial and tangential direction
s	Height of the squealer rim measured from the base of the untreated tip section, (Figure 10)

SQA33 Partial squealer rim with $t/h=1.03\%$ and $(t-s)/t=1/3$ The shortest rim in the chordwise direction

SQC33 Partial squealer rim with $t/h=1.03\%$ and $(t-s)/t=1/3$ The longest rim in the chordwise direction

SQC66 Partial squealer rim with $t/h=1.03\%$ and $(t-s)/t=2/3$ The longest rim in the chordwise direction

SSSq-A The shortest partial squealer rim, Config A

SSSq-B Mid-sized partial squealer rim, Config B

SSSq-C The longest partial squealer rim, Config C

t Rotor tip clearance height without any squealer rim.

TE Trailing edge

$(t-s)/t$ Effective clearance height between squealer rim top plane and outer casing

U_m Mean wheel speed at rotor mid-span

τ_{max} blade maximum thickness

w Squealer rim width w=4 mm

V Absolute velocity

W Relative velocity with respect to turbine rotor

x,y,z Coordinate system for the numerical analysis (axial,tangential, radial direction in a linear cascade arrangement)

X,Y,Z,T Flow visualization planes used for numerical laser sheet visualizations (see Figure 4)

z/t Distance between the plane of visualization and the tip platform (see Figure 3)

REFERENCES

Camei,C., Dey, D.,Kavurmacioglu, L., 2003, “ Tip Leakage Flows near Partial Squealer Rims in an Axial Flow Turbine Stage,” ASME GT2003-38979, paper presented at the ASME IGTI Turbo Expo held in Atlanta, Georgia, June 2003.

Chen,G., Dawes,W.N., and Hodson,H.P., 1993, “A Numerical Investigation of Tip Gap Flow,” AIAA 93-2253, presented at the AIAA/SAE/ASME/ASEE 29th Joint Propulsion Conference and Exhibit.

Heyes, F.J.G. and Hodson, H.P., Dailey, G.M, 1992, “The Effect of Blade Tip Geometry on the Tip Leakage Flow in Axial Turbine Cascades,” ASME Journal of Turbomachinery, Vol.114, pp.643-651.

Kavurmacioglu,L., Dey,D. and Camci,C., 2004, "Tip Leakage Flow Simulation in AFTRF (Axial Flow Turbine Research Facility) Blade Passages," VKI Lecture Series on "Turbine Blade Tip Design and Tip Clearance Treatment" 19-23 January 2004, pp. 27-41.

Lakshminarayana,B., Camci,C., Halliwell,I., and Zaccaria,M., 1992, "Investigation of Three Dimensional Flow Field in a Turbine Including Rotor/Stator Interaction. Part I: Design Development and Performance of the Research Facility," AIAA paper 92-3326, presented at the ASME-AIAA Joint Propulsion Conference, Nashville, Tennessee.

Launder,B.E. and Spalding,D.B, 1974, "The Numerical Computation of Turbulent Flows," Comp.Meth.Appl.Mech. Eng.Vol.3,pp-269-28.

Lin, Y.L., Shih, T.I.P., Chyu, M.K. and Bunker, R.S., 2000, "Effects of Gap Leakage on Fluid Flow in a Contoured Turbine Nozzle Guide Vane," ASME paper 2000-GT-0555.

Liu, J. and Bozzola, R., 1993, "Three-Dimensional Navier-Stokes Analysis of Tip Clearance Flow in Linear Turbine Cascades," AIAA Journal, Vol.31, pp.2068-2074.

Sell, M., Treiber, M., Casciaro, C. and Gyarmathy, G., "Tip-clearance-affected Flow Fields in a Turbine Blade Row," Proc. Inst. Mech. Eng., Vol.213, Part A, pp.309, 318.

Tallman, J. and Lakshminarayana, B., 2001, " Numerical Simulation of Tip Leakage Flows in Axial Flow Turbines, with Emphasis on Flow Physics: Part I – Effect of Tip Clearance Height," ASME Journal of Turbomachinery, Vol.123, pp.314-323.

Tallman, J. and Lakshminarayana, B., 2001, " Numerical Simulation of Tip Leakage Flows in Axial Flow Turbines, with Emphasis on Flow Physics: Part II – Effect of Outer Casing Relative Motion," ASME Journal of Turbomachinery, Vol.123, pp.324-333.

VKI Lecture Series on " Turbine Blade Tip Design and Tip Clearance Treatment" 19-23 January 2004, pp. 1-26.

Wisler, D.C., 1985, "Aerodynamic Effects of Tip Clearance, Shrouds, Leakage Flow, Casing Treatment, and Trenching in Compressor Design" Von Karman Institute Lecture Series 1985-05 on Tip Clearance Effects in Axial Turbomachinery,".